Imaging Assessment of Primary Prostate Cancer, Focused on Advanced MR Imaging and PET/CT

Jin Hee Jang[1], Jae Young Byun[1], Minsung Kim[1], Young Joon Lee[1], Sun Nam Oh[1], Sung Eun Rha[1], Ie-Ryung Yoo[2]

Imaging assessment of prostate cancer is one of the most difficult sections of oncology imaging. Detecting, localizing and staging of the primary prostate cancer by preoperative imaging are still challenging for the radiologist. Magnetic resonance (MR) imaging provides excellent soft tissue contrast and is widely used for solid organ imaging, but results of preoperative imaging of the prostate gland with conventional MR imaging is unsatisfactory. Positron emission tomography and computed tomography (PET/CT) is the cornerstone in oncology imaging, but some limitations prohibit the assessment of primary prostate cancer with PET or PET/CT. Recent studies to overcome these insufficient accuracies of imaging evaluation of primary prostate cancers with advanced MR techniques and PET and PET/CT are reported. In this article, we review the imaging findings of prostate cancer on variable modalities, focused on MR imaging and PET/CT.

Index words : Prostate cancer
Oncologic imaging
MRI technique
PET/CT

Introduction

Imaging assessment of prostate cancer has a very important role for the management of patients with diagnosed or suspected prostate cancer. At the same time, imaging of prostate cancer is one of the most difficult sections of oncology imaging and still challenging for the radiologist. Transrectal ultrasound (TRUS), magnetic resonance (MR) imaging, and computed tomography (CT) are the most commonly and widely used modalities for preoperative staging, guidance for biopsy or treatment, and postoperative follow-up (1, 2). But reported sensitivity and specificity of these conventional modalities are unsatisfactory (1–5). To overcome insufficient accuracies of these conventional modalities, the advanced MR imaging and combined positron emission tomography and computed tomography (PET/CT) are recruited. In this review, we will discuss imaging findings of prostate

JKSMRM 12:89-99(2008)
[1]Department of Radiology, Kangnam St. Mary's Hospital, College of Medicine, The Catholic University of Korea.
[2]Department of Nuclear Medicine, Kangnam St. Mary's Hospital, College of Medicine, The Catholic University of Korea.
Received; September 20, 2008, accepted; October 31, 2008
Corresponding author : Jae Young Byun, M.D., Department of Radiology, Kangnam St. Mary's Hospital, College of Medicine, The Catholic University of Korea, 505 Banpo-dong, Seocho-gu, Seoul 137-701, South Korea
Tel. 82-2-590-2785, 2468 Fax. 82-2-599-6771 E-mail: jybyun@catholic.ac.kr

cancer on variable imaging modalities, focused on MR imaging and PET/CT.

Transrectal ultrasound

Generally, prostate cancer shows nonspecific findings on TRUS. Prostate cancer in the peripheral zone is usually seen as a hypoechoic mass (Fig. 1) on TRUS (6). Mass with bulging or irregular contour on TRUS suggests extracapsular extension, and length of the contact of lesion with prostate gland is associated with the probability of extracapsular invasion (7). In the MR imaging era, the clinical role of TRUS is limited to assess volume of prostate gland for prostate specific antigen (PSA) density, and guidance for systemic biopsy, targeted-extraprostatic biopsy or brachytherapy.

Computed tomography

Evaluating the intraprostatic anatomy of the prostate gland and extraprostatic involvement with CT is limited and not recommended. Small prostate cancer is poorly defined on CT scan. Only some large tumors can be delineated on CT. The role of CT in clinical practice is in assessing nodal staging, distant metastasis, and baseline study for locally advanced disease (i.e. gross extracapsular disease, gross seminal vesicle invasion, or invasion of surrounding structures including bladder, rectum, levator ani muscles or pelvic floor) and these are beyond the coverage of this review.

Conventional MR imaging

Reported accuracies of the prostate cancer detection of MR imaging are widely variable and guideline for the indications of MR imaging in the patients with diagnosed or suspected prostate cancers still has controversies (1–5). Generally, MR imaging of the prostate gland is helpful in patients with negative TRUS-guided biopsy in spite of high PSA value, or in patients with biopsy-proven prostate cancer for preoperative staging. Hemorrhage after biopsy limits the accuracy of prostate MR imaging, so a delay of 6-8 weeks between biopsy and MR imaging is needed (8 - 10). Optimal image resolution is acquired by high tesla (more than 1.5T) magnet machine combined with pelvic phased-array coil and endorectal coil. MR imaging with endorectal coil provides better images with increased spatial resolution and contrast in demonstrating contour of tumor and assessment of extraprostatic invasion. But problems induced by endorectal coil, such as patient's discomfort, near field artifact, artifact by peristalsis, distortion of images of peripheral zone by ballooning of probe, should be considered.

Conventional MR imaging for the prostate gland includes (a) the axial sagittal spin echo or fast spin echo

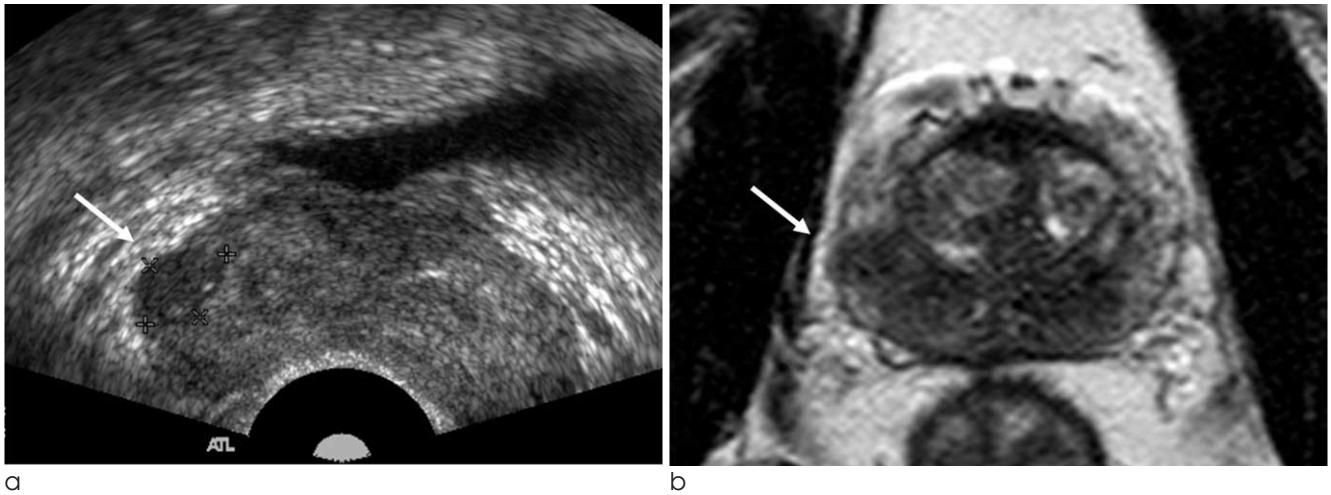

a b

Fig. 1. Prostate cancer with extracapsular involvement on TRUS
TRUS (a) of a 67-year-old male patient with high PSA level (37.9 ng/mL) shows a 1.2×1.0 cm sized, relatively well-defined hypoechoic mass (arrow) with bulging contour in right peripheral zone. Axial T2-weighted image of similar section (b) shows a small hypointense nodule (arrow) with bulging contour in right peripheral zone. Capsular surface overlying low SI nodule is poorly differentiated with periprostatic fat. Radical prostatectomy was performed, and prostate cancer with extracapsular invasion (T3, Gleason's score 7) was confirmed in right peripheral zone.

T1-weighted images (TR 400-500, TE 10-15), (b) axial, sagittal and coronal spin echo or fast spin echo T2-weighted images (TR 3500-4000, TE 130-140), and (c) contrast enhanced axial and coronal T1-weighted images with or without fat saturation. Especially thin (3-mm) slice and a small field of view are helpful in evaluation of local staging including the extraprostatic involvement (3).

On T1-weighed images, both prostate parenchyma and prostate cancer appear as homogeneous intermediate signal intensity (SI). Hence, T1-weighted images are used for assessment of pelvic lymph nodes and pelvic bones, rather than primary prostate cancer. Hemorrhage after previous biopsy is seen as high SI on T1-weighted images (Fig. 2), which is helpful to differentiate the post-biopsy hemorrhage and prostate carcinomas, both are seen as low SI on T2-weighted images.

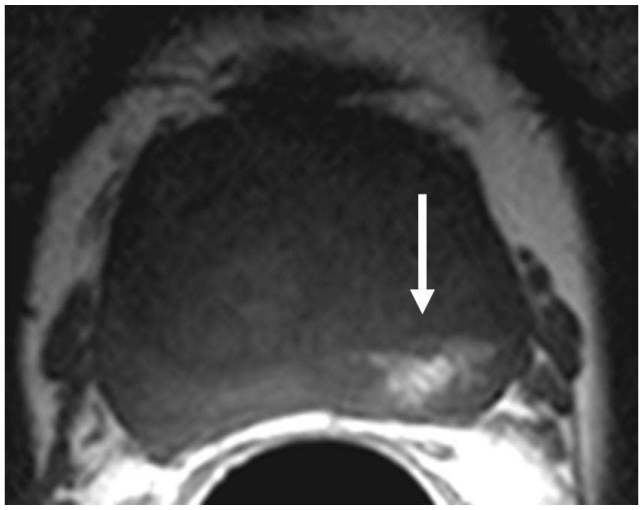

Fig. 2. Post-biopsy hemorrhage on T1-weighted image
Axial T1-weighted image after outside prostate biopsy shows patchy hyperintensity (arrow) in left peripheral zone, suggesting post-biopsy hemorrhage.

On T2-weighted images, the prostate cancer in peripheral zone is seen as low SI (Fig. 1, 3), in contrast with high SI of normal peripheral zonal parenchyma (11). Most prostate cancer arises from the peripheral zone, so T2-weighted images have a major role in the detection of prostate cancer. But, some benign conditions such as prostatitis and hemorrhage can be seen as focal low SI within peripheral zone; hence correlation with other sequence is needed. For this purpose, scanning axial T1- and T2-weighted imaging of prostate gland with the same slice thickness and field of view for alignment of the two sequences is helpful. Involvement of prostatic capsule, extraprostatic fat, neurovascular bundles, seminal vesicle and bladder base are assessed with T2-weighted images (Fig. 4, 5, and 6). In cases with extraprostatic invasion, local staging of prostate cancer is T3 or T4, which means the less chance for curative surgical treatment (12, 13).

Normal parenchyma of the transition zone shows low SI on T2-weighted image (Fig. 7), which makes difficult

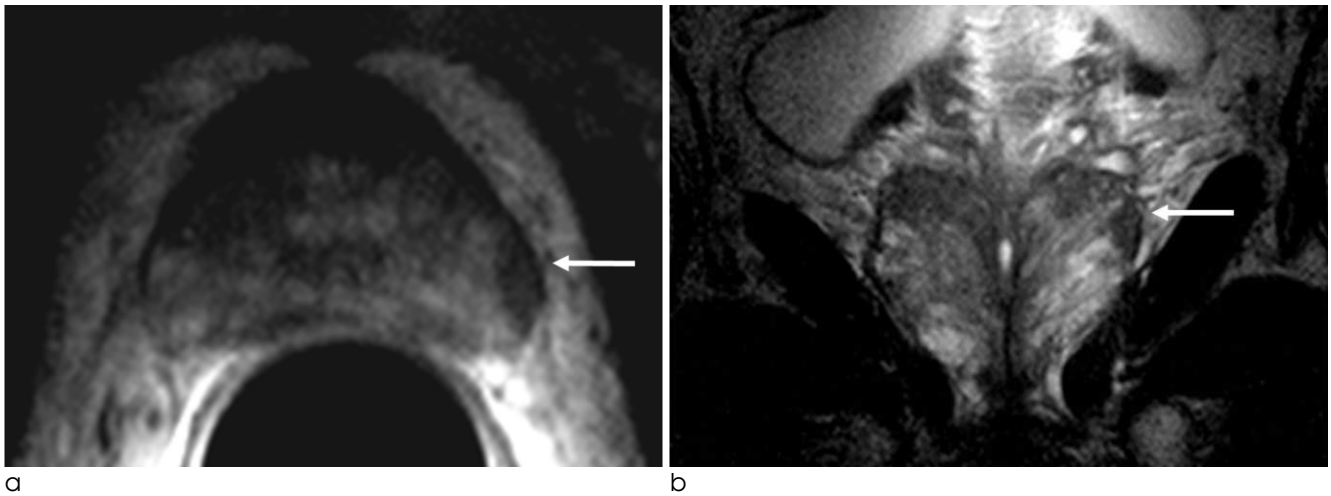

a b

Fig. 3. Prostate cancer on conventional T2-weighted image
Axial T2-weighted image (a) shows a small hypointense nodule (arrow) in the subcapsular portion of left peripheral zone. Coronal T2-weighted image (b) shows well-demarcated hypointense lesion (arrow) in left peripheral zone. Note the intact hypointense capsule on T2-weighted image. A small adenocarcinoma (Stage T2, Gleason's score 7) in left peripheral zone was surgically confirmed.

Fig. 4. Extracapsular invasion
An ovoid hypointense nodule (arrow) is seen in right peripheral zone on axial T2-weighted image. Margin of the mass is poorly defined (double arrows) and dark signal capsule is not seen in right lateral aspect of the mass, as compared with intact capsule (arrowheads) on contralateral side of prostate. Findings are compatible with prostate cancer in right peripheral zone with extracapsular invasion. Prostate cancer with extracapsular invasion (T3, Gleason's score 6) was confirmed by radical prostatectomy.

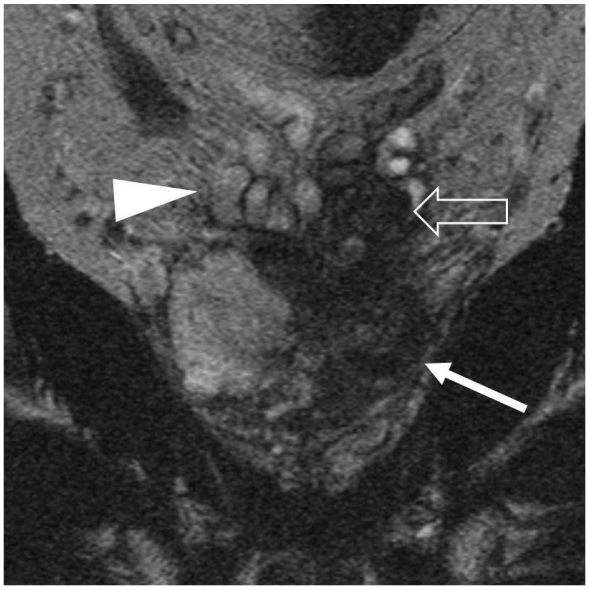

Fig. 6. Seminal vesicular invasion
Coronal T2-weighted image reveals the irregular shaped hypointense mass (arrow) involving the left peripheral zone of prostate gland with extension into seminal vesicle superiorly. Normal high signal intensity of seminal vesicle (arrowhead) is replaced by low signal intensity mass (open arrow). Radical prostatectomy found the prostate cancer in left peripheral zone with seminal vesicular invasion, which means local staging as T3b.

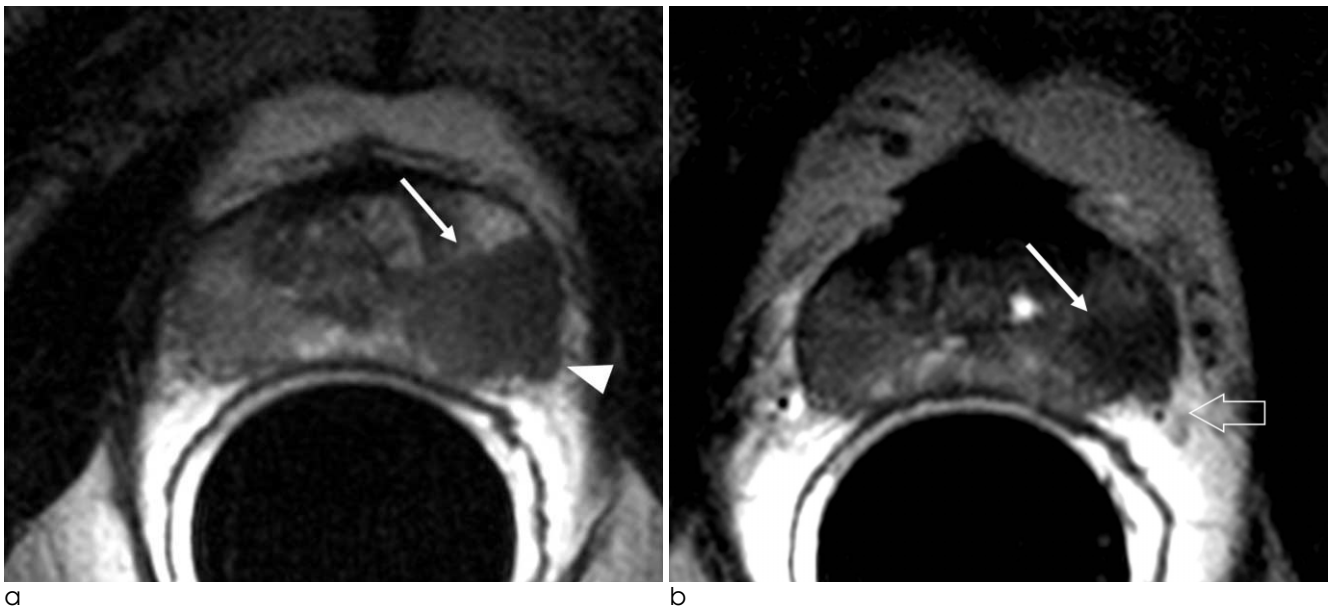

a b

Fig. 5. Neurovascular bundle invasion
Two serial axial T2-weighted images of prostate gland show a nodular hypointense mass (arrows) in the mid-portion of left peripheral zone on axial T2-weighted images (a and b). Focal bulging contour (arrowhead) with obliteration of low SI capsule and indistinct margin between mass and adjacent fat suggests extracapsular invasion. Axial T2-weighted image of lower level (b) discloses nodular bulging, contacting with the neurovascular bundle (open arrow). Note the intact right side of prostatic capsule and right neurovascular bundle. Surgical specimen disclosed neurovascular bundle invasion by prostate cancer.

to detect cancers in the transition zone. Findings helpful in detecting cancers in the transition zone are followings; [a] homogenous low SI on T2-weighted image, [b] ill-defined or spiculated margin, [c] deficit of low SI rim which is characteristic of benign adenoma, [d] obliteration of surgical pseudocapsule (transition zone-to-peripheral zone boundary of low SI), [e] urethral or anterior fibromuscular stromal invasion, [f] lenticular-shaped lesion (14).

Dynamic contrast-enhanced MR Imaging

Prostate cancer has increased vascularity like other malignant tumors, and it is probably due to neovascularization and increased interstitial space (15). These pathological characteristics are associated to more rapid enhancement of prostate cancer after intravenous contrast agent than normal parenchyma (Fig. 8). Because the normal prostate parenchyma is vascular, more rapid injection and rapid scanning of prostate gland are required to detect the increased vascularity of prostate cancer. After intravenous infusion of a full dose of gadolinium chelate (0.1 mmol/kg) injected at 3 ml/sec, serial 3D acquisitions of prostate gland are required for assessment of enhancement pattern of prostate lesion. Generally 3D T1-weighted spoiled gradient echo sequence is used

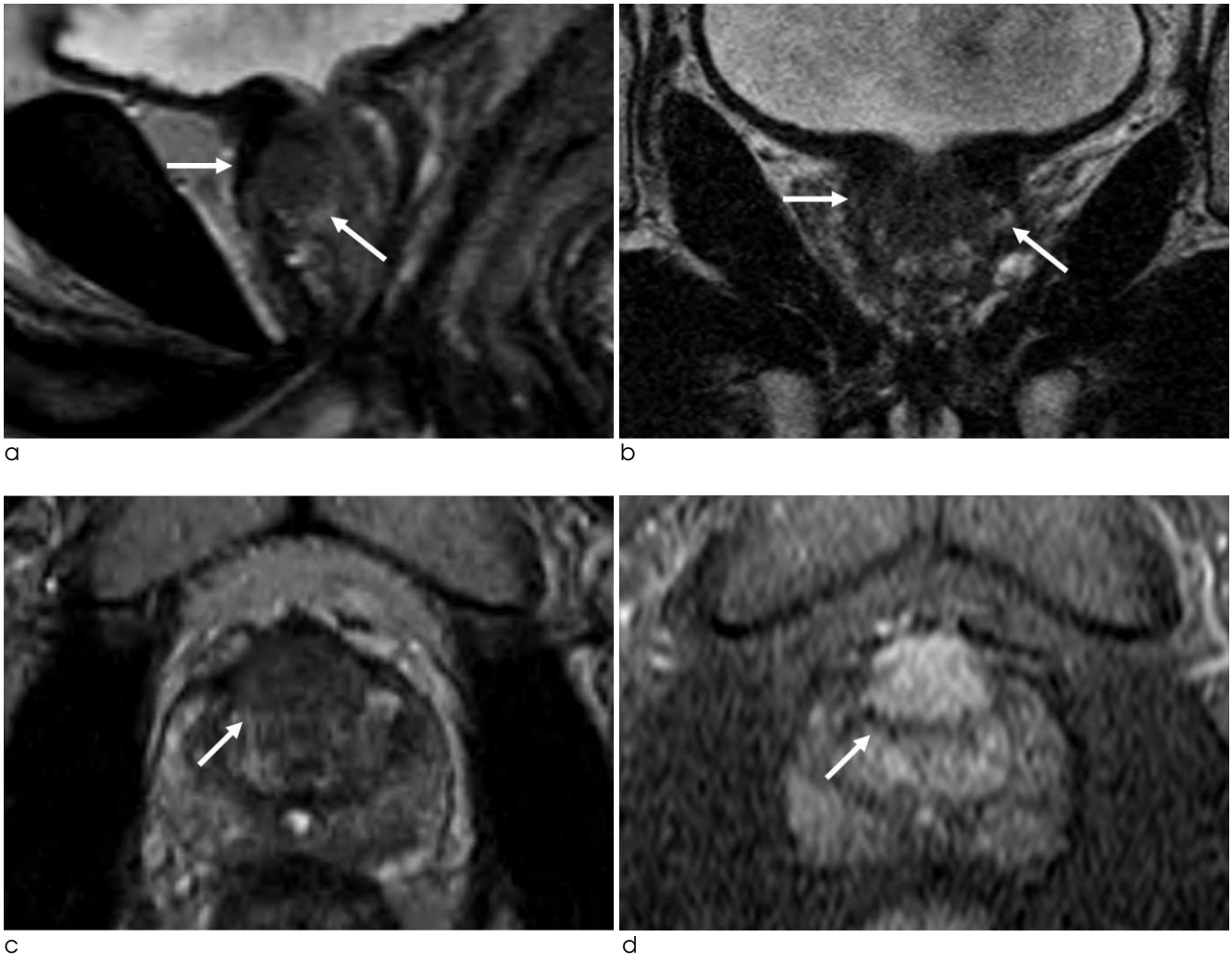

Fig. 7. Prostate cancer in transitional zone
On sagittal and coronal T2-weighted images (a and b) of prostate gland, a homogenous hypointense mass (arrows) is noted in transitional zone. On axial T2-weighted image (c), margin of the mass (arrow) is poorly defined without discernible low signal intensity rim. At 30 seconds after intravenous contrast infusion (d), early nodular enhancement of the mass (arrow) is seen. Adenocarcinoma involving transitional zone with extracapsular invasion (T3, Gleason score 7) was surgically confirmed.

and images are acquired serially with 5 to 10 seconds interval. Reports about the dynamic contrast-enhanced MR imaging of prostate cancers with high tesla machine showed considerable outcomes for detecting and localizing the prostate cancers (16, 17). Direct inspection of images, color mapping of variable perfusion parameters, and signal intensity curves of region-of-interest are used for analysis of enhancement patterns. But analyses of dynamic contrast-enhanced MR imaging and its results remain controversial, so further studies are needed.

Diffusion-weighted image

Diffusion-weighted image (DWI) reflects the diffusion coefficient of the tissue, using the additional diffusion gradients. DWI is widely used for detection of cytotoxic edema of hyperacute or acute infarction of brain (18). Clinical application of DWI is extended, as a promising method for detection and localization of malignant tumors (19, 20). As well as other cancer cells, prostate cancer shows restricted diffusion and decreased apparent diffusion coefficient (ADC) value (Fig. 9), due to high cellularity, enlargement of nuclei, hyperchromatisms and angulations of the nuclear contour (21, 22). Contrast of the cancer from normal prostate parenchyma is associated primarily with the difference of ADC values between the cancer and normal parenchyma, and the individual variability of

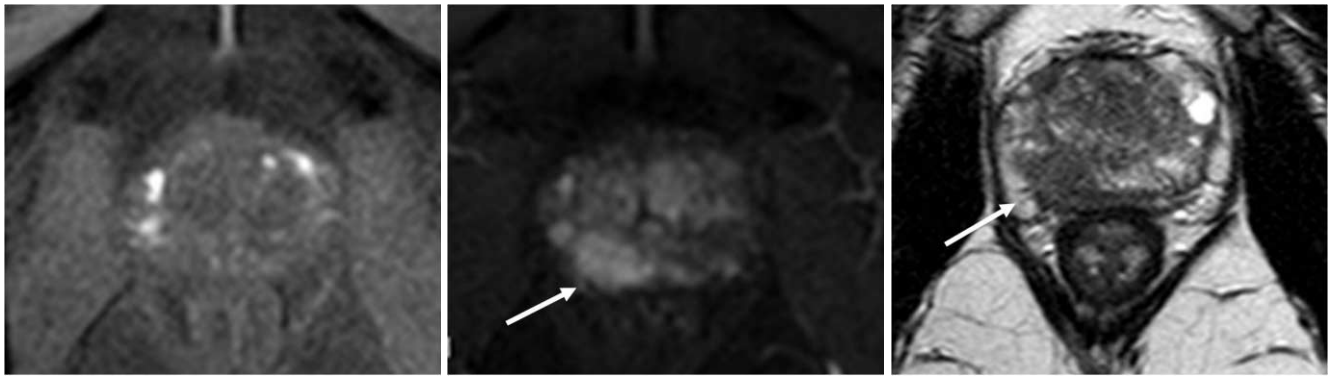

a b c

Fig. 8. Dynamic contrast-enhanced MR Imaging
Dynamic contrast-enhanced MR imaging of prostate gland of same patient in Figure 4 was performed. Precontrast image (a) shows no focal lesion. At 30 seconds after intravenous contrast infusion, focal area in right peripheral zone (arrow) shows stronger enhancement than other prostate parenchyma (b). Axial T2-weighted image (c) shows same location and size of tumor with dynamic contrast enhancement study.

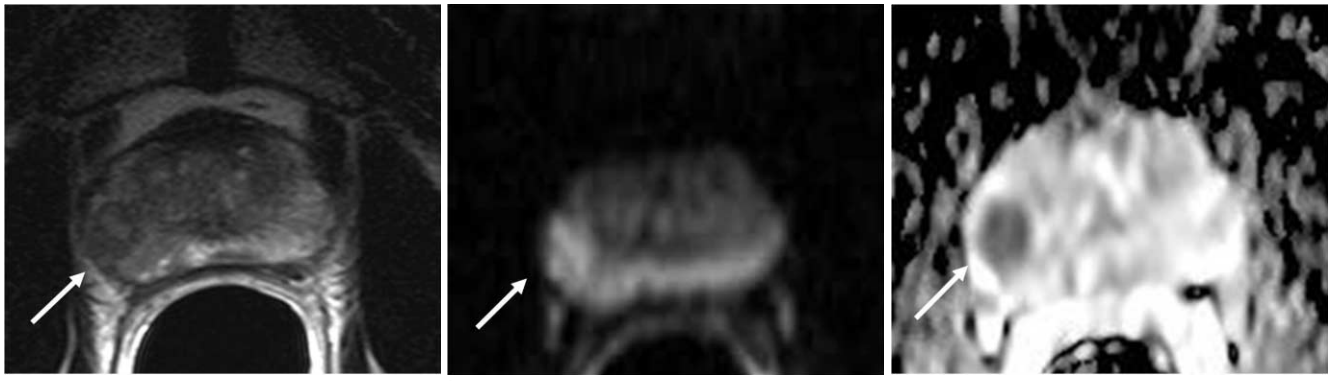

a b c

Fig. 9. Diffusion-weighted image
Axial T2-weighted image (a) shows oval hypointense mass (arrow) in right peripheral zone. DWI (b=1000, b) shows increased SI of mass with decreased ADC value (c), suggesting diffusion restriction. Radical prostatectomy was done, and adenocarcinoma (T2, Gleason's score 9) in right peripheral zone was confirmed. (Reprinted with permission, from reference 2)

ADC values is another factor for the ADC values (22–25). Recent reports suggest the diagnostic value of DWI, conjunction with other imaging modalities (22, 25, 26). Also high tesla MR units can make the difference of ADC value wider than conventional MR units (27). There is no consensus about the b value of the DWI of prostate gland, but recent studies used the b value from 800 to 1000 (28, 29). DWI of prostate is acquired by gradient-echo echo-planar images, which is one of the most fast imaging sequences of MR. Short acquisition time is another advantage of DWI.

MR spectroscopy

MR spectroscopy provides metabolic information about prostatic tissue by displaying the relative concentrations of chemical compounds within contiguous small volumes of interest (voxels). Three-dimensional proton MR spectroscopic metabolic mapping of the entire gland is possible with a resolution of 0.24 mL. Normal prostate glandular parenchyma has relatively high concentration of citrate due to citrate-producing metabolism. MR spectroscopy of prostate cancer reveals decreased level of citrate and increased

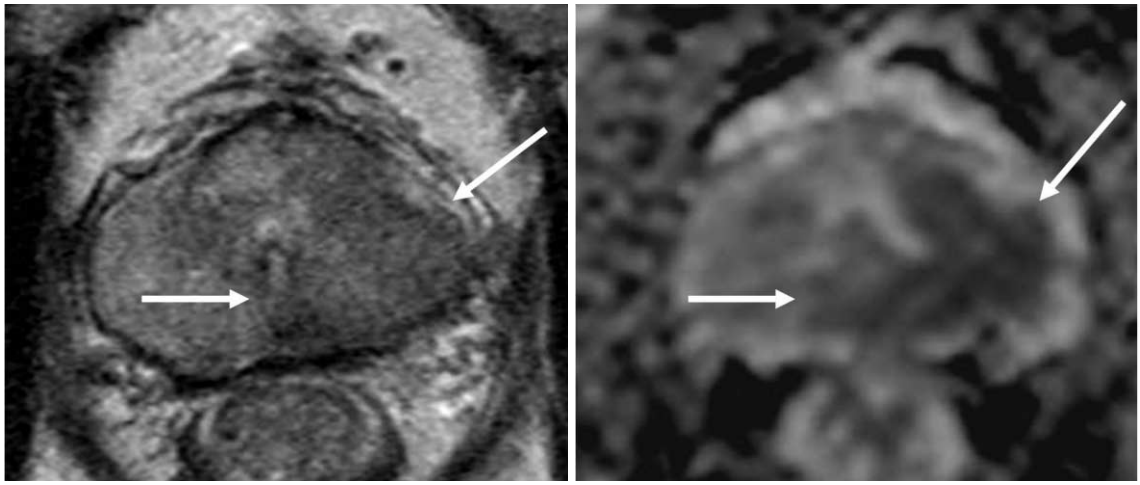

a b

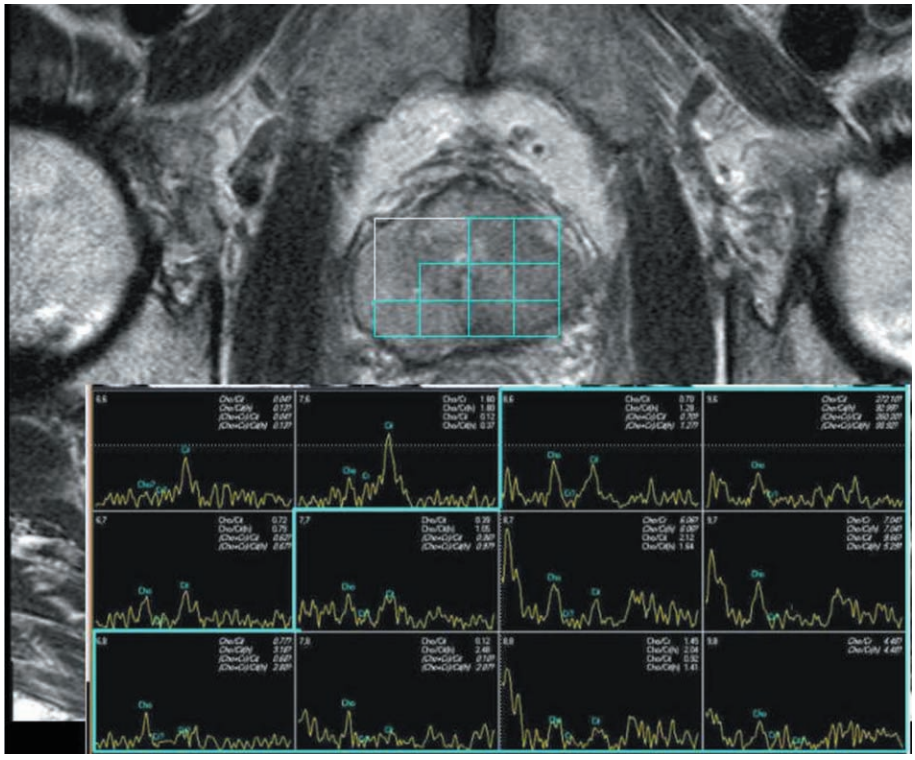

c

Fig. 10. MR spectroscopy
T2-weighted image (a) shows subtle hypointense lesion (arrows) in left peripheral zone and transitional zone. ADC map (b) shows decreased ADC value in the corresponding area (arrows). Multi-voxel 3D MR spectroscopy at midgland level (c) reveals the increased choline peak and decreased citrate peak at corresponding area (green box) of prostate cancer. Total acquisition time was within 9 minutes (TR/TE 800/140 msec). (Courtesy of Dr. BK Park, Samsung Medical Center, Seoul, Korea)

level of choline, which represent the accelerated cell membrane turnover (Fig. 10). So we can localize the prostate cancer with MR spectroscopy, with increased accuracy in detecting and localizing prostate cancer (3, 30-32). Another distinguishing feature of MR spectroscopy is the assessment of metabolic characteristic of neoplasm. Some reports suggest MR spectroscopy can predict the aggressiveness and treatment response of tumor (32). These are helpful to estimate the prognosis of patients with prostate cancer with MR spectroscopy.

PET and PET/CT

PET and PET/CT are whole body imaging modalities based on the detection of annihilation photons released when specific radionuclides emit positrons that undergo annihilation with electrons (33). Radiopharmaceuticals of PET and PET/CT are composed of isotopes emitting positron and metabolic surrogates that participates into the metabolic pathway. PET/CT fuses the metabolic information of PET scan on the anatomical frame of CT, so results in more accurate localization of uptake and improved diagnostic accuracy than PET alone.

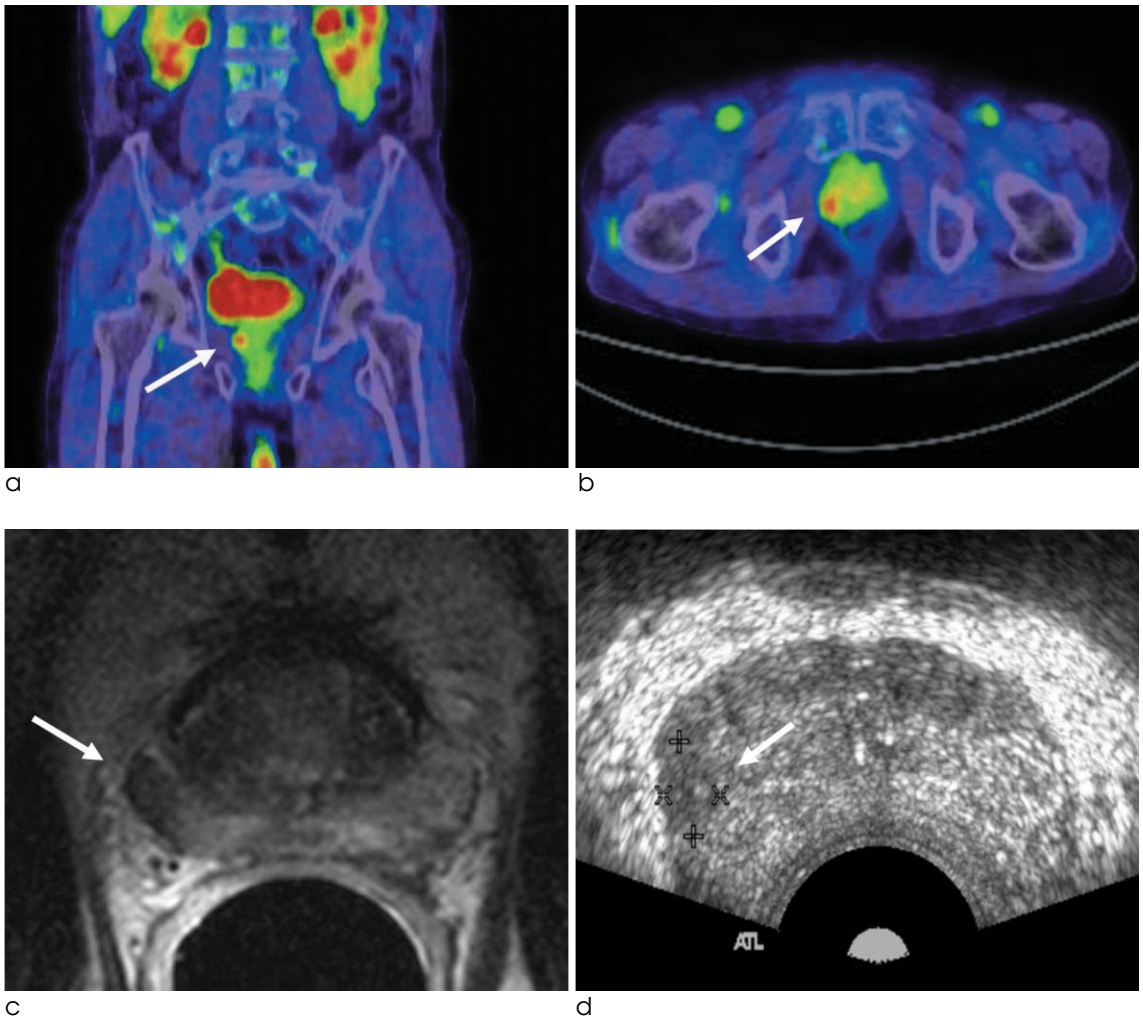

Fig. 11. Prostate cancer detected on PET/CT

A 74-year-old male patient with malignant sarcoma in right nasal cavity had been performed PET/CT for restating after surgical removal of tumor. Note a nodular moderate FDG uptake (max and mean SUV 3.3/2.8, arrow) in just inferior aspect of FDG collection within the urinary bladder on fusion images of PET/CT (a and b). In this circumstance, differential diagnosis for this nodular FDG uptake includes primary malignant nodule, metastatic nodule, or even benign hyperplastic nodule. Serum PSA level is moderately increased (5.7 ng/mL). Axial T2-weighted image (c) reveals nodular hypointense mass (arrow) in right peripheral zone. TRUS (d) shows nodular hypoechoic mass (arrow) on right peripheral zone. Transrectal biopsy was performed under TRUS guidance, ad adenocarcinoma of prostate gland, with Gleason score 6 was found.

Variable positron emitters are used for PET and PET/CT. Among those radionuclides, ^{18}F-deoxyglucose (^{18}F -FDG) is most widely used and available in common clinical settings. FDG is an analogue of glucose and ^{18}F -FDG PET detects the tissues with facilitated glucose metabolism and assesses the glucose metabolic activity of tissue semi-quantitatively (33). Most malignant tumor showed increased uptake and utilization of glucose, due to increased metabolic demands (34). Hence, we can find the tumors with increased glucose metabolism with ^{18}F-FDG PET and PET/CT. Vice versa, detection and localization of tumors with decreased or slightly increased glucose metabolism with ^{18}F -FDG PET and PET/CT is difficult.

Well-differentiated prostate cancer utilizes less glucose than other malignant tumors, so less ^{18}F -FDG uptake than others (Fig. 11). ^{18}F -FDG is excreted via kidneys and accumulated in the bladder, just above the prostate gland (35). This accumulation can mask the subtle uptake of prostate cancer. Also, benign hyperplastic nodules of prostate gland and inflammation such as prostitis casue uneven hot uptake of prostate background parenchyma, which also can mask or mimic the uptake of prostate cancer. These difficulties make the sensitivity of ^{18}F -FDG PET for prostate cancer low, so ^{18}F -FDG PET for prostate cancer has a limited role for assessing the primary prostate cancer (36–39).

Other metabolic tracers containing ^{11}C are alternative to increase the accuracy of PET for prostate cancer. However, ^{11}C has very short half-life, which limits the clinical application of these materials. ^{11}C -choline is used for synthesis of phospholipid, hence can be used as another marker for cellular proliferation (40). A recent report comparing the ^{11}C -choline PET and MR imaging/spectroscopy shows that PET is more accurate regarding the localization of main primary prostate cancer lesion than MR imaging/spectroscopy (41). In this report, they suggest that ^{11}C -choline PET reflects tumor volume rather than tumor grade. But benign prostate hyperplasia and prostatitis may cause high uptake of ^{11}C -choline. Another study on a small series of patients reported that the statistically insignificant difference of uptake on ^{11}C -choline PET between the prostate cancer and benign hyperplastic nodules, but a tendency towards higher values in carcinoma was noted (40). ^{11}C -acetate can be used as an indicator of tumor growth, because of acetate is associated with active basal lipid metabolism which is a part of cell membrane synthesis (42). Acetate is not excreted via urinary system and shows lower physiologic uptake around the pelvic cavity than FDG. Sandblom et al suggest value of PET with ^{11}C -acetate in detecting and localizing after radical prostatectomy (43). PET with ^{11}C -methionine may represents increased amino acid transport and metabolism, and a recent report suggests the diagnostic value of PET with ^{11}C-methionine in androgen-resistant prostate cancer (44).

Conclusion

Prostate cancers show variable imaging findings according to the imaging modalities. Hence, imaging assessment of prostate cancer is very difficult and approach with multiple imaging modalities is essential. MR imaging has a critical role in preoperative imaging assessment in patients with prostate cancer. Application of dynamic contrast enhancement, DWI and MR spectroscopy are the promising methods for detecting and characterizing the prostate cancers. Also, PET/CT could be another cornerstone for staging and localizing the prostate cancer.

References

1. Hricak H, Choyke PL, Eberhardt SC, Liebel SA, Scardino PT. Imaging prostate cancer: a multidisciplinary perspective. Radiology 2007;243:28-53.
2. 변재영. 전립선 암의 다양한 영상과 전망. Radiology Digest 2007;2:8-18.
3. Hricak H, White S, Vigneron D, Kurhanewicz J, Kosco A, Levin D, et al. Carcinoma of the prostate gland: MR imaging with pelvic phased-array coils versus integrated endorectalpelvic phased-array coils. Radiology 1994;193: 703-709.
4. Scheidler J, Hricak H, Vigneron DB, Yu KK, Sokolov DL, Huang LR, et al. Prostate cancer: localization with three-dimensional proton MR spectroscopic imaging-clinicopathologic study. Radiology 1999;213:473-480.
5. Kim JK, Hong SS, Choi YJ, Park SH, Ahn H, Kim CS, et al. Wash-in rate on the basis of dynamic contrast-enhanced MRI: usefulness for prostate cancer detection and localization. J Magn Reson Imaging 2005;22:639-646.
6. Shinohara K, Wheeler TM, Scardino PT. The appearance of prostate cancer on transrectal ultrasonography: correlation of imaging and pathological examinations. J Urol 1989;142:76-82.
7. Ukimura O, Troncoso P, Ramirez EI, Babaian RJ. Prostate

cancer staging: correlation between ultrasound determined tumor contact length and pathologically confirmed extraprostatic extension. J Urol 1998;159:1251-1259.
8. Ikonen S, Kivisaari L, Vehmas T, Tervahartiala P, Salo JO, Taari K,et al. Optimal timing of post-biopsy MR imaging of the prostate. Acta Radiol 2001;42:70-73.
9. White S, Hricak H, Forstner R, Kurhanewicz J, Vigneron DB, Zaloudek CJ, et al. Prostate cancer: effect of postbiopsy hemorrhage on interpretation of MR images. Radiology 1995;195:385-390.
10. Qayyum A, Coakley FV, Lu Y, Olpin JD, Wu L, Yeh BM, et al. Organ-confined prostate cancer: effect of prior transrectal biopsy on endorectal MRI and MR spectroscopic imaging. AJR Am J Roentgenol 2004;183:1079-1083.
11. Schnall MD, Pollack HM. Magnetic resonance imaging of the prostate gland. Urol Radiol 1990;12:109-114.
12. Lu-Yao GL, McLerran D, Wasson J, Wennberg JE. An assessment of radical prostectomy. Time trends, geographic variation, and outcomes, The Prostate Patient Outcomes Research Team. JAMA 1993;269:2633-2636.
13. Fleming C, Wasson JH, Albertsen PC, Barry MJ, Wennberg JE. A decision analysis of alternative treatment strategies for clinically localized prostate cancer. The Prostate Patient Outcomes Research Team. JAMA 1993;269:2650-2658.
14. Akin O, Sala E, Moskowitz CS, Kuroiwa K, Ishill NM, Pucar D, et al. Transition zone prostate cancers: features, detection, localization, and staging at endorectal MR imaging. Radiology 2006;239:784-792.
15. Buckley DL, Roberts C, Parker GJ, Logue JP, Hutchinson CE. Prostate cancer: evaluation of vascular characteristics with dynamic contrastenhanced T1-weighted MR imaging-initial experience. Radiology 2004;233:709-715.
16. Jager GJ, Ruijter ET, van de Kaa CA, de la Rosette JJ, Oosterhof GO, Thornbury JR, et al. Dynamic TurboFLASH subtraction technique for contrast-enhanced MR imaging of the prostate: correlation with histopathologic results. Radiology 1997;203:645-652.
17. Kim CK, Park BK, Kim B. Localization of prostate cancer using 3T MRI: comparison of T2-weighted and dynamic contrast-en- hanced imaging. J Comput Assist Tomogr 2006;30:7-11.
18. Warach S, Gaa J, Siewert B, Wielopolski P, Edelman RR. Acute human stroke studied by whole brain echo planar diffusion-weighted magnetic resonance imaging. Ann Neurol 1995;37:231-241.
19. Tien RD, Felsberg GJ, Friedman H, Brown M, MacFall J. MR imaging of high-grade cerebral gliomas: value of diffusion-weighted echoplanar pulse sequences. AJR Am J Roentgenol 1994;162: 671-677.
20. Eis M, Els T, Hoehn-Berlage M. High resolution quantitative relaxation and diffusion MRI of three different experimental tumors in rat. Magn Reson Med 1995;34:835-844.
21. Anderson JR. Muir's textbook of pathology. London, England: Edward Arnold, 1985.
22. Sato C, Naganawa S, Nakamura T, Kumada H, Miura S, Takizawa O, et al. Differentiation of noncancerous tissue and cancer lesions by apparent diffusion coefficient values in transition and peripheral zones of the prostate. J Magn Reson Imaging 2005;21:258-262.
23. Gibbs P, Tozer DJ, Liney GP, Turnbull LW. Comparison of quantitative T2 mapping and diffusion- weighted imaging in the normal and pathologic prostate. Magn Reson Med 2001;46:1054-1058.
24. Issa B. In vivo measurement of the apparent diffusion coefficient in normal and malignant prostatic tissues using echo-planar imaging. J Magn Reson Imaging 2002;16:196-200.
25. Hosseinzadeh K, Schwarz SD. Endorectal diffusion- weighted imaging in prostate cancer to differentiate malignant and benign peripheral zone tissue. J Magn Reson Imaging 2004;20:654-661.
26. Shimofusa R, Fujimoto H, Akamata H, Motoori K, Yamamoto S, Ueda T, et al. Diffusion-weighted imaging of prostate cancer. J Comput Assist Tomogr 2005;29:149-153.
27. Gibbs P, Pickles MD, Turnbull LW. Diffusion imaging of the prostate at 3.0 tesla. Invest Radiol 2006;41:185-188.
28. Choi YJ, Kim JK, Kim N, Kim KW, Choi EK, Cho KS. Functional MR imaging of prostate cancer. Radiographics 2007;27:63-75.
29. Mazaheri Y, Shukla-Dave A, Hricak H, Fine SW, Zhang J, Inurrigarro G, et al. Prostate cancer: identification with combined diffusion-weighted MR imaging and 3D 1H MR spectroscopic imaging--correlation with pathologic findings. Radiology 2008;246:480-488.
30. Jung JA, Coakley FV, Vigneron DB, Swanson MG, Qayyum A, Weinberg V, et al. Prostate depiction at endorectal MR spectroscopic imaging: investigation of a standardized evaluation system. Radiology 2004;233:701-708.
31. Coakley FV, Kurhanewicz J, Lu Y, Jones KD, Swanson MG, Chang SD, et al. Prostate cancer tumor volume: measurement with endorectal MR and MR spectroscopic imaging. Radiology 2002;223:91-97.
32. Zakian KL, Sircar K, Hricak H, Chen HN, Shukla-Dave A, Eberhardt S, et al. Correlation of proton MR spectroscopic imaging with Gleason score based on step-section pathologic analysis after radical prostatectomy. Radiology 2005;234:804-814.
33. Kapoor V, McCook BM, Torok FS. An introduction to PET-CT imaging. Radiographics 2004; 24:523-543.
34. Smith TA. FDG uptake, tumor characteristics and response to therapy: a review. Nucl Med Commun 1998; 19:97-105.
35. Sanz G, Robles JE, Gimenez M, Arocena J, S?nchez D, Rodriguez-Rubio F, et al. Positron emission tomography with 18fluorine- labelled deoxyglucose: utility in localized and advanced prostate cancer. BJU Int 1999;84:1028-1031.
36. Effert PJ, Bares R, Handt S, Wolff JM, Bull U, Jakse G. Metabolic imaging of untreated prostate cancer by positron emission tomography with 18fluorine-labeled deoxyglucose. J Urol 1996;155:994-998.
37. Hofer C, Laubenbacher C, Block T, Breul J, Hartung R, Schwaiger M. Fluorine-18-fluorodeoxyglucose positron emission tomography is useless for the detection of local recurrence after radical prostatectomy. Eur Urol 1999;36:31-

35.
38. Liu IJ, Zafar MB, Lai YH, Segall GM, Terris MK. Fluorodeoxyglucose positron emission tomography studies in diagnosis and staging of clinically organ-confined prostate cancer. Urology 2001;57:108-111.
39. E. Salminen, A. Hogg and D. Binns Frydenberg M, Hicks R. Investigation with FDG-PET scanning in prostate cancer show limited value for clinical practice. Acta Oncol 2002;41:425-429.
40. Sutinen E, Nurmi M, Roivainen A, Varpula M, Torvanen T, Lehikoinen P, et al. Kinetics of [11C]choline uptake in prostate cancer: a PET study. Eur J Nucl Med Mol Imaging 2004;31:317-324.
41. Yamaguchi T, Lee J, Uemura H, Sasaki T, Takahashi N, Oka T, et al. Prostate cancer: a comparative study of 11C-choline PET and MR imaging combined with proton MR spectroscopy. Eur J Nucl Med Mol Imaging 2005;32:742-748.
42. Yoshimoto M, Waki A, Yonekura Y, Sadato N, Murata T, Omata N, et al. Characterization of acetate metabolism in tumor cells in relation to cell proliferation acetate metabolism in tumor cells. Nucl Med Biol 2001;28:117-122.
43. Sandblom G, Sörensen J, Lundin N, Häggman M, Malmström PU. Positron emission tomography with C11-acetate for tumor detection and localization in patients with prostate-specific antigen relapse after radical prostatectomy. Urology 2006;67:996-1000.
44. Macapinlac HA, Humm JL, Akhurst T, Osman I, Pentlow K, Shangde C, et al. Differential Metabolism and Pharmacokinetics of L-[1-(11)C]-Methionine and 2-[(18)F] Fluoro-2-deoxy-D-glucose (FDG) in Androgen Independent Prostate Cancer. Clin Positron Imaging 1999;2:173-181.

대한자기공명의과학회지 12:89-99(2008)

자기공명영상과 PET/CT를 중심으로 한 전립선 암의 영상 진단

[1]강남성모병원 영상의학과, [2]강남성모병원 핵의학과

장진희[1] · 변재영[1] · 김민성[1] · 이영준[1] · 오순남[1] · 나성은[1] · 유이령[2]

전립선 암은 종양 영상 분야에서 가장 어려운 분야 중 하나이다. 술전 영상 검사를 통한 전립선 암의 발견(detection), 정위 (localization) 그리고 병기결정(staging)은 여전히 영상의학과 의사의 도전이 필요한 분야이다. 자기공명 영상은 우수한 연부 조직 대조를 보이며 여러 고형 장기의 영상에 널리 쓰이나, 전립선의 술전 자기공명 영상의 결과는 기대에 미치지 못한다. 전산화단층촬영 영상과 결합된 양전자방출단층촬영술 (PET/CT)은 종양 영상의 발달에 획기적인 기여를 하였으나, 전립선암의 평가에는 어려움이 많다. 최근에 이러한 불충분한 정확도를 극복하기 위하여 발전된 자기공명 영상 기법과 PET/CT을 이용한 전립선암 영상에 대한 연구들이 발표되었다. 본 종설에서는 새로운 기법의 자기 공명 영상과 PET/CT 영상을 중심으로 전립선암의 다양한 영상 기법과 그 소견을 살펴볼 것이다.

통신저자 : 변재영, (137-701) 서울시 서초구 반포동 505, 강남성모병원 영상의학과
Tel. (02) 590-2785, 2468 Fax. (02) 599-6771 E-mail: jybyun@catholic.ac.kr